THE JOURNAL OF PHYSICAL CHEMISTRY C

Article

pubs.acs.org/JPCC

Molecular Design of a Room-Temperature Maser

Stuart Bogatko,[*,†,‡,¶] Peter D. Haynes,[†,§] Juna Sathian,[†] Jessica Wade,[§,∥] Ji-Seon Kim,[§,∥] Ke-Jie Tan,[†] Jonathan Breeze,[†] Enrico Salvadori,[⊥,#] Andrew Horsfield,[†,‡,¶] and Mark Oxborrow[†]

[†]Department of Materials, Imperial College London, Exhibition Road, London SW7 2AZ, U.K.

[‡]London Centre for Nanotechnology, Department of Materials, Imperial College London, Exhibition Road, London SW7 2AZ, U.K.

[¶]Thomas Young Centre, Imperial College London, Exhibition Road, London SW7 2AZ, U.K.

[§]Department of Physics, Imperial College London, Exhibition Road, London SW7 2AZ, U.K.

[∥]Centre for Plastic Electronics, Imperial College London, Exhibition Road, London SW7 2AZ, U.K.

[⊥]London Centre for Nanotechnology, University College London, 17-19 Gordon Street, WC1H 0AH, London, U.K.

[#]School of Biological and Chemical Sciences, Queen Mary University of London, Mile End Road, E1 4NS, London, U.K.

Supporting Information

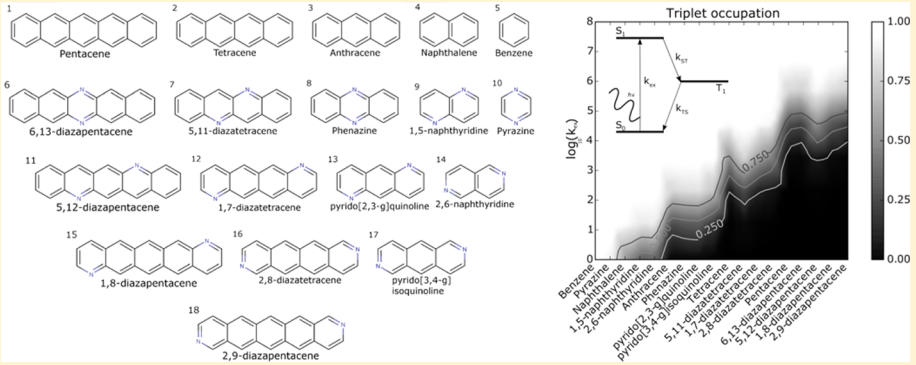

ABSTRACT: A computational molecular design strategy, complemented by UV/vis absorption and time-resolved electron paramagnetic resonance (EPR) spectra measurements, is employed to guide the search for active molecules for a room-temperature maser that can achieve continuous-wave operation. Focusing on linear polyacenes and diaza-substituted forms, our goal is to model how important maser properties are influenced by acene length and location of nitrogen substitution. We find that tetracene, its diaza-substituted forms (5,11-, 1,7-, and 2,8-diazatetracene), and anthracene possess singlet to triplet intersystem crossing rates highly favorable toward masing. The diaza-substituted forms of pentacene (6,13-, 5,12-, 1,8-, and 2,9-diazapentacene) also stand out as ideal candidates due to their similarity to the working pentacene prototype. A steady-state population analysis suggests the working conditions under which continuous-wave masing can be achieved for these molecules. Operational frequencies are estimated from calculated zero field splitting parameters.

INTRODUCTION

The maser is the microwave analogue of the laser, renowned for enabling high-quality amplifiers with exceptional performance. However, to date the maser has been limited in application due to the high vacuum and low temperatures needed for it to function. A maser capable of operating continuously under ambient conditions without the need for large magnetic fields, vacuum pumps, and cryogenic cooling systems would immediately revolutionize the domains of microwave communication and electron paramagnetic resonance (EPR) spectroscopy by enabling high precision measurements such as for biological structure determination. The recent discovery of an organic molecular crystal based maser operating in pulsed mode at room temperature[1,2] constituted a dramatic step forward toward this goal. However, achieving continuous-wave operation requires optimization of the active molecule, which is laborious experimentally. This paper reports the results of a computational molecular design strategy based upon a combination of first principles and empirical methods that has enabled this search to be accelerated and its scope to be widened.

The pentacene/*p*-terphenyl based room-temperature maser operates as follows (see Figure 1a). The pentacene molecules are optically excited from the S_0 ground singlet state into the S_1 singlet state by a short laser pulse near 590 nm. The electrons in the S_1 state rapidly undergo an intersystem crossing (ISC) facilitated by spin−orbit coupling into the triplet manifold arriving first at the T_2 state with a spin-selected population inversion of the T_X, T_Y, and T_Z sublevels with a ratio of

Received: January 6, 2016
Revised: February 23, 2016
Published: March 29, 2016

DOI: 10.1021/acs.jpcc.6b00150
J. Phys. Chem. C 2016, 120, 8251−8260

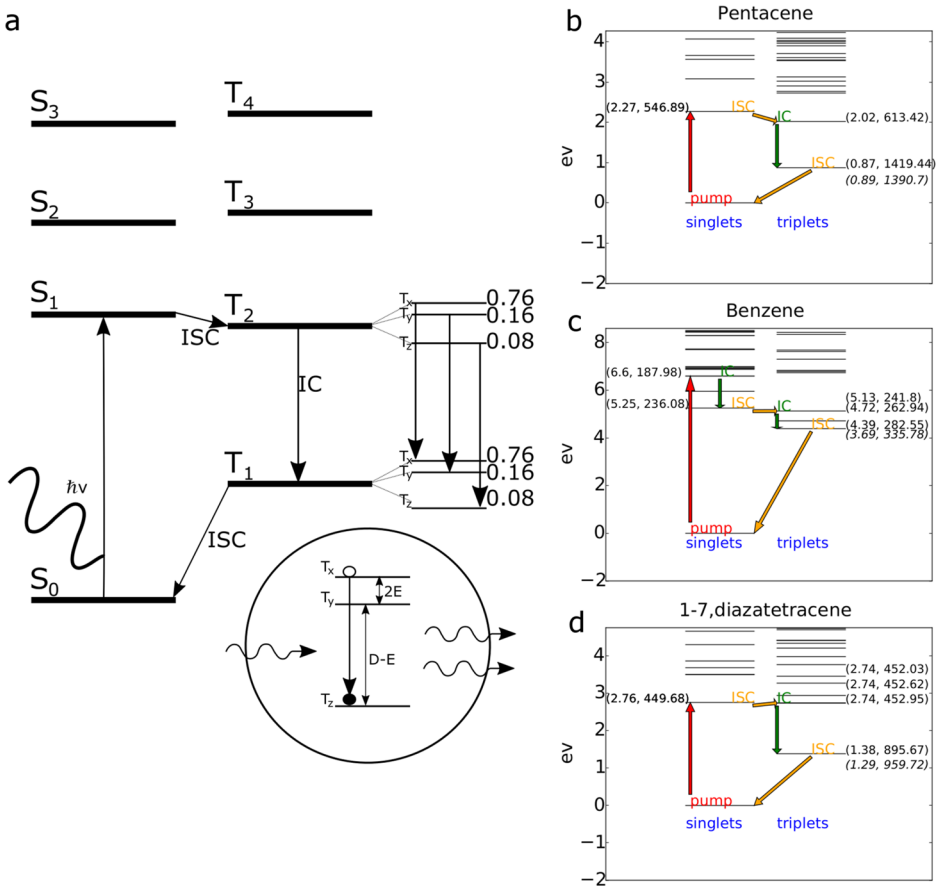

Figure 1. Schematic diagram of the of the maser process in the pentacene in *p*-terphenyl prototype maser (a); the excited state structure computed in this work with relevant transitions indicated: pump laser excitation (red), ISC (yellow), and IC (green) for pentacene (b), benzene (c), and 1,7-diazatetracene (d). Energies (nm, eV) are provided in parentheses relative to S_0; italics indicate energies wherein the geometry was optimized for the T_1 state.

0.76:0.16:0.08.[3,4] The electrons (spins) in the T_2 state rapidly relax to the T_1 state via internal conversion (IC) while preserving this population inversion. A final ISC from T_1 to S_0 provides a spin-flushing mechanism, bringing the electron back to the ground state. While the T_1 state is populated, however, it is possible to stimulate a transition from the X to Z sublevels (see inset in Figure 1a) or from the X to Y sublevels. Because the splitting of these levels is in the microwave regime, this process results in the stimulated emission of microwave radiation. With the construction of a suitable resonator cavity, a significant amplification of microwave photons can be achieved.[1,2]

Following the initial development of the pentacene doped *p*-terphenyl prototype maser, an important next step involves the search for materials that can improve operation and add new functionality. It is of central interest to construct a continuous-wave (CW) room-temperature maser. This goal remains elusive using the current configuration of the pentacene/*p*-terphenyl prototype because electrons accumulate in the T_Z state, blocking further masing. Some have proposed new materials, in particular silicon carbide and diamond with nitrogen-vacancy defects, which may operate as a CW room-temperature maser though have yet to be realized.[5,6] This work presents the results of a computational search of organic materials, the linear polyacenes and selected diaza-substituted forms, aimed at proposing new maser materials especially those which may operate as a CW maser. The focus on these molecules is motivated by their similarities to the pentacene prototype, the only known working room-temperature maser. The excited state electronic structure of the linear polyacenes, of which pentacene is a member, are governed by $\pi-\pi$ and $\sigma-\pi$ transitions. As a result of this, the linear polyacenes possess roughly similar excited state properties, the differences being due to the number of acene rings.[7] The choice of nitrogen substitution is based on the observation that ISC in N-substituted linear polyacenes can be accelerated relative to unsubstituted forms.[8] The goal of this work is thus to model how important maser properties are influenced by acene length and location of nitrogen substitution in order to more effectively direct the materials discovery process for the room-temperature maser.

We are thus in need of a calculation method which allows for rapid evaluation of molecular properties for the linear polyacenes and their derivatives. Our main concern is to understand conceptual changes in electronic structure properties of candidate molecules with the purpose of predicting their usefulness as the active molecule in a room-temperature maser device. Our focus is specifically on S_0-S_1, S_1-T_n, T_1-S_0 transition energies and zero field splitting (ZFS) of the T_1 state. Treatment of population inversion (see discussion of Figure 1a), which requires accurate estimates of the contributions of the T_X, T_Y, and T_Z sublevels to the S_1-T_n ISC rate, is not attempted in this work. Producing an accurate theoretical description of the excited state electronic structure of the linear polyacenes is known to be quite difficult. In cases where, for example, highly accurate excitation energies are required,

DOI: 10.1021/acs.jpcc.6b00150
J. Phys. Chem. C 2016, 120, 8251−8260

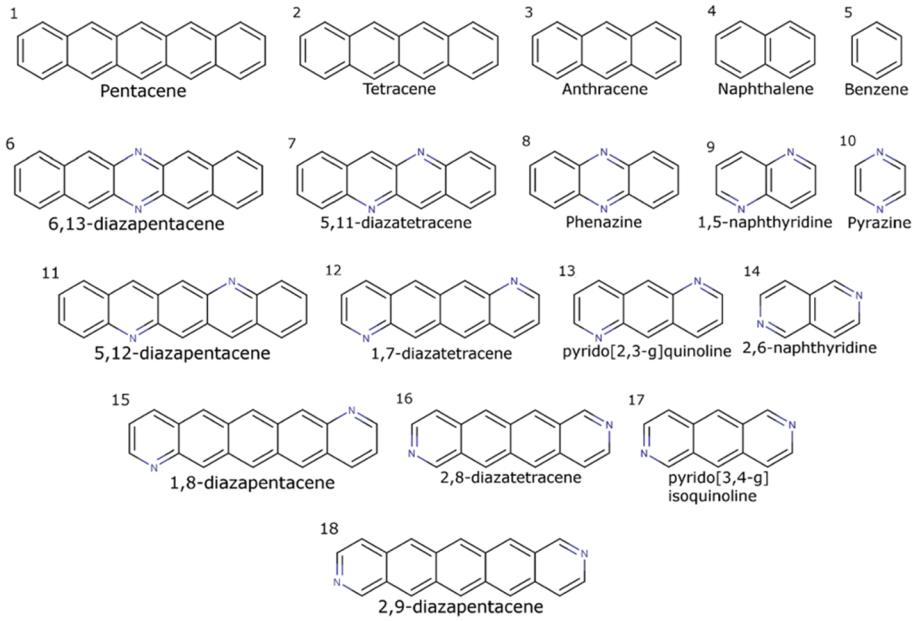

Figure 2. List of acenes and diazaacenes used in this study. Compound numbers appear on the top-left of each molecule.

researchers often turn to multireference methods with perturbative corrections; see, for example, the recent work of Zimmerman et al.[9] High level multireference methods are too computationally demanding for a rapid screening process. It would be more efficient to proceed with a lower level of theory to screen out the majority of candidates. Such a solution is provided by density functional theory (DFT) and time dependent DFT (TDDFT) where the many-body quantum problem is simplified considerably in exchange for computational feasibility of the ground and excited state electronic structure, respectively.[10−13]

METHODS

There are known difficulties associated with the application of DFT and TDDFT to the linear polyacenes. The nature of the lowest lying singlet excited state, S_1, changes as acene length increases. For naphthalene S_1 is an L_b-type state wherein polarization is along the long molecular axis while those of anthracene and the larger polyacenes are L_a-type states wherein polarization is along the short molecular axis. TDDFT predicts this transition between L_b and L_a states to occur earlier, relative to acene length, than is observed.[14,15] Furthermore, Gastel discusses a spin polarization effect which influences ZFS parameters.[16] We tackle these errors by comparing selected results with experimental data, allowing us to formulate empirical corrections. The resulting methodology provides a successful mixture of the efficiency of TDDFT with the accuracy of experimental observation. Our final results suggests that this is a sound, qualitative approach which will provide a considerable reduction in computational and experimental overhead costs as well as an overall speedup of the materials discovery process.

The 18 acenes and diazaacenes investigated in this study are shown in Figure 2. Geometry optimizations of the ground state singlet were performed using DFT[10,13,17,18] with the PBE exchange correlation (XC) functional[19] and the cc-pvqz basis set.[20] The excited state electronic structure was obtained using TDDFT[11,12] and the same XC functional and basis sets as with the DFT calculation. Two sets of calculations were performed to generate the lowest 25 singlet and 25 triplet excited states using the lowest lying singlet (here the true ground state) and lowest triplet state, respectively, as a reference state in the TDDFT calculation. The results of these calculations were used to estimate S_0-S_1 and S_1-T_n transition energies. A second set of DFT calculations were performed wherein the molecular geometry was optimized for the lowest triplet state electron configuration followed by a single point energy calculation in the ground state S_0 electron configuration. These energies were used to estimate the T_1-S_0 transition energies under the assumption that the molecular geometry relaxes while in the T_1 state as a result of its long lifetime. Geometry optimizations were performed in vacuum while ground and excited state electronic structure calculations were performed in vacuum and in the presence of a polarizable continuum model (PCM)[21] used to represent the *p*-terphenyl-like host. This was achieved by setting static and optical dielectric constants to those of *p*-terphenyl, 5760 and 2.86, respectively,[22,23] while keeping the remaining parameters set to those of benzene. This choice of solvent is motivated by the pentacene/*p*-terphenyl system being the only working room-temperature maser in existence. All DFT and TDDFT calculations discussed above were performed using the Gaussian 09 software suite.[24]

ZFS parameters *D* and *E* were evaluated for the T_1 state using the ORCA computational chemistry software[25] using the formalism developed by Neese and co-workers.[26] The geometry of each molecule was optimized in the triplet ground state electronic configuration using the PBE XC functional and the cc-pvdz basis set using the resolution of the identity (RI) approximation and split valence auxiliary basis[27] before the ZFS parameters were evaluated. The cc-pvdz basis set was here chosen because larger basis sets offered no improvement in the calculated *D* and *E* parameters (see the Supporting Information).

Singlet excitation energies of linear polyacenes computed via TDDFT are known to deviate from available experimental data.[14,28] We have observed that the triplet excitation energies also exhibit errors relative to available experimental data, albeit of smaller magnitude. ZFS parameters are similarly found to deviate from experimental data.[16,29] It has been argued that these errors arise from DFT's poor ability to describe large π-electron systems.[14] The error is systematic, however, and Gastel et al. have

DOI: 10.1021/acs.jpcc.6b00150
J. Phys. Chem. C 2016, 120, 8251−8260

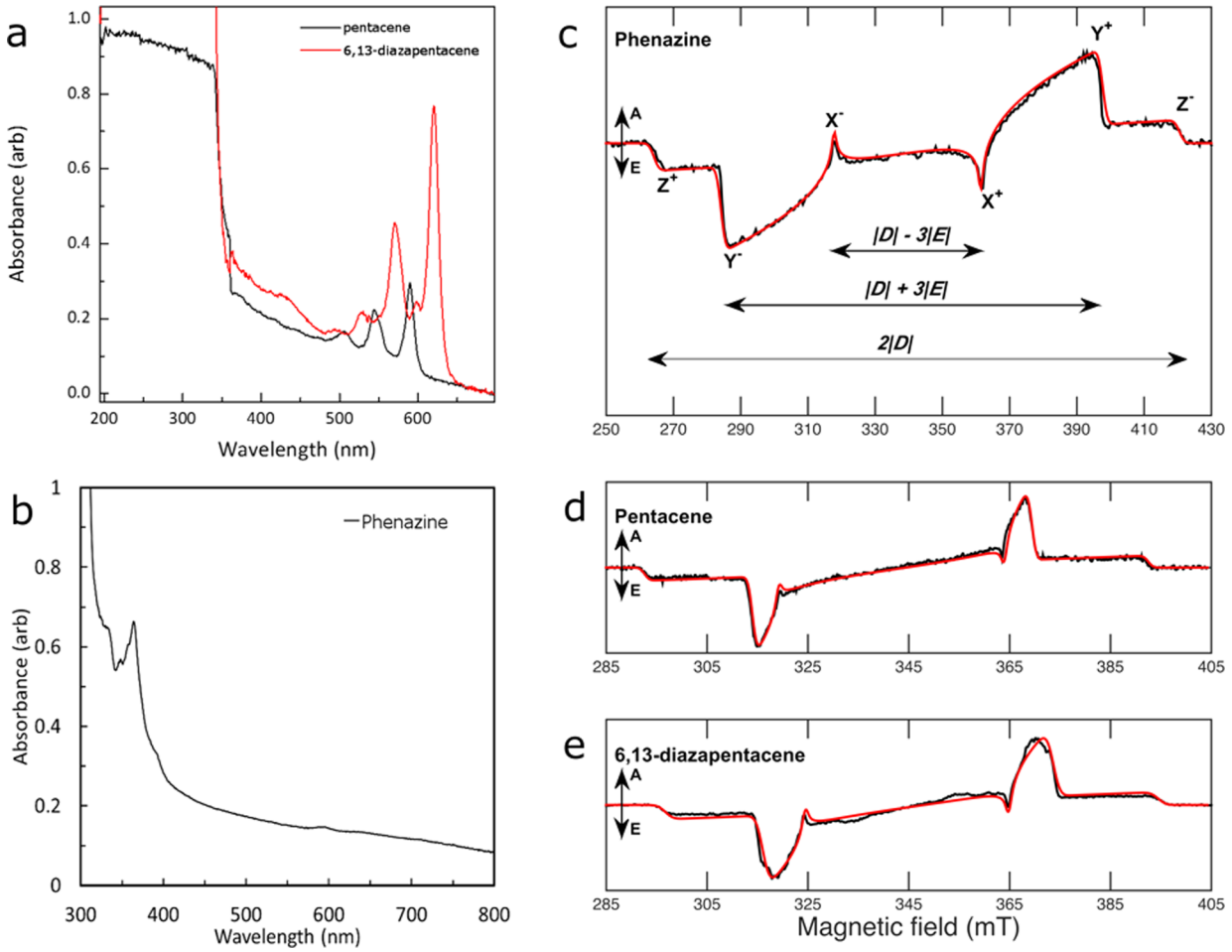

Figure 3. Experimental UV−vis and EPR measurements. UV/vis spectra of pentacene and 6,13-diazapentacene in *p*-terphenyl (a) and phenazine in biphenyl (b). TR-EPR (black lines) and relative simulations (red lines) of powder samples of phenazine in biphenyl and pentacene and 6,13-diazapentacene in *p*-terphenyl recorded at 9 GHz at room temperature (panels c, d, and e). The simulations were performed with Easyspin[47] with parameters reported in Table S1. Panel c reports the canonical field positions and equations used to derive the ZFS parameters *D* and *E* directly from the experimental data, sublevel energy order $P_X > P_Y > P_Z$. Phenazine was excited at 355 nm, and the pentacene and 6,13-diazapentacene were excited at 590 and 532 nm, respectively. A = enhanced absorption, E = emission.

postulated an empirical equation describing the error as a function of the number of π-electrons or, alternatively, the number of carbons in their linear polyacene molecular systems.[16] Here we take a similar approach in the formulation of empirical corrections to our calculated properties that essentially amounts to applying correcting functions obtained from linear fits of curves comparing DFT calculated values to experimental observations found in the literature[28,30−42] for the S_0−S_1 and T_1−S_0 energy splittings and the ZFS parameters *D* and *E*; these corrections are described in detail in the Supporting Information. Along similar lines, empirical equations describing ISC rates are obtained by comparing DFT computed energy gaps to published ISC rates.[43−46] No empirical corrections for the S_1−T_n energy splittings were performed since there is no direct experimental data available. Because we are also concerned with the effect of nitrogen substitution and because the number of π-electrons is conserved under such substitutions, we assume that the correcting functions constructed from linear polyacene data can be transferred to the diazaacenes. As described below, our empirically corrected data is validated against three experimental controls, pentacene and 6,13-diazapentacene in *p*-terphenyl and phenazine in biphenyl, that indicate that this method is qualitatively correct.

Crystals of pentacene and 6,13-diazapentacene in a *p*-terphenyl host lattice and phenazine in biphenyl were grown using an open system zone melting method,[2] and the results of experimental characterization are shown in Figure 3. UV−visible absorption spectra of the pentacene/*p*-terphenyl and 6,13-diazapentacene/*p*-terphenyl samples were acquired using a Shimadzu UV-2550 spectrophotometer while those of phenazine/biphenyl were acquired using an Agilent Cary 5000 UV−vis−NIR spectrophotometer. ZFS parameters were obtained from simulation of X-band time-resolved EPR spectra of powder samples.The measurements were performed on a Bruker E580 pulsed EPR spectrometer equipped with a Bruker dielectric ring resonator (ER 4118X-MD5). Spectra were recorded in direct detection mode with disabled magnetic field modulation; this allows direct observation of the characteristic enhanced absorptive (A) and emissive (E) lines. The optical excitation was provided by a Surelite broadband OPO system (operating range 410−680 nm), pumped by a Surelite I-20 Q-switched Nd:YAG laser with second and third harmonic generators (20 Hz, pulse length: 5 ns). EPR spectra were simulated using the EasySpin[47] toolbox in MATLAB.

DOI: 10.1021/acs.jpcc.6b00150
J. Phys. Chem. C 2016, 120, 8251−8260

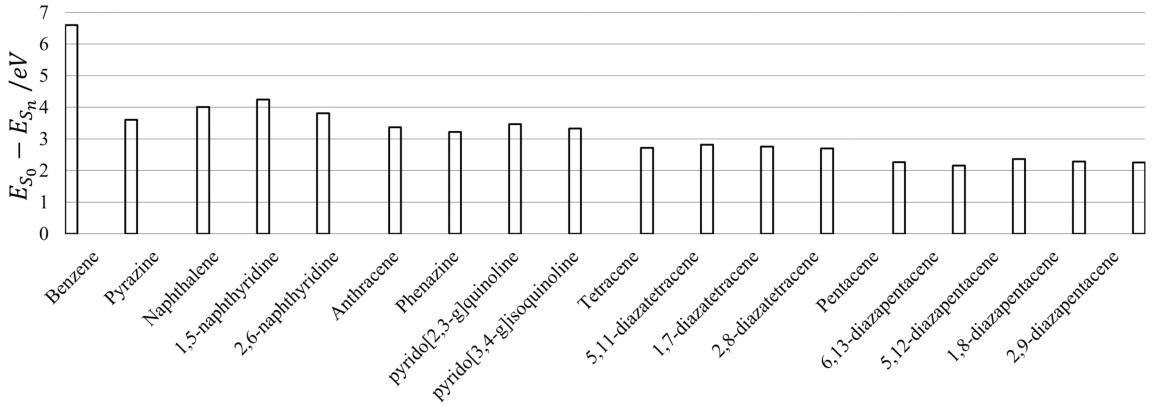

Figure 4. Empirically corrected (for DFT errors; *vide supra*) excitation energies for all molecules in a *p*-terphenyl-like host (estimated error is ~0.2 eV).

RESULTS

Energy level diagrams are shown in Figures 1b, 1c, and 1d that summarize our results. The following electronic transitions are identified: (1) the pump excitation from the singlet ground state to the lowest lying absorbing singlet (that is, with nonzero oscillator strength), (2) the S_1-T_n ISC transitions between the lowest lying excited singlet state and the nearest downhill triplet state, (3) IC transitions between the triplet state involved with the S_1-T_n ISC and T_1, and (4) a final (spin-flushing) T_1-S_0 ISC bringing the electron back to the ground state. The schematics for all maser candidate molecules are provided in the Supporting Information. Two excitation pathways to S_1 exist: pumping directly to the lowest lying singlet (as we observe for pentacene in Figure 1b) or to a higher lying singlet coupled with an additional IC to S_1 (as we observe for benzene, Figure 1c). Furthermore, the number of triplet states in proximity to S_1 can be quite large such as for 1,7-diazatetracene (Figure 1d), where our results indicate three triplet states near to S_1. In the following we consider the S_0-S_1, S_1-T_n, and T_1-S_0 transitions and the ZFS parameters of T_1 in more detail.

Singlet Excitation. The maser process is initiated via optical excitation by a pump laser whereby an electron is excited from S_0 to a low lying excited singlet state. For all cases studied, the excitation is in excess of 2 eV and, because the maser process itself involves an emission in the μeV regime (i.e., 10^{-6} eV), there remains an immense amount of energy which is transferred to the crystal host as heat via nonradiative IC and ISC transitions. As such, there is an obvious disadvantage for molecules requiring larger excitation energies because these would be accompanied by significantly more heating during operation. The excitation energies are provided in Figure 4 for each molecule in order of increasing size and diaza substitution in order of increasingly outward facing position. A trend of decreasing photoabsorption energy as acene length increases is clearly visible in Figure 4 and is in fact a well-known trend in linear polyacenes.[7] Diaza substitution, on the other hand, has not been so thoroughly studied. The effects of nitrogen substitution are non-negligible, and their effect appears as regular, small variations in the excitation energies relative to nitrogen position suggesting a relatively minor influence on the structure of the singlet excited state manifold.

UV–visible absorption spectra have been measured for three samples, pentacene in *p*-terphenyl, 6,13-diazapentacene in *p*-terphenyl, and phenazine in biphenyl. Analysis of these spectra indicates absorption energies of 2.10 eV, 2.00 eV, and 3.41 eV for the lowest optical transitions for pentacene and 6,13-diazapentacene in *p*-terphenyl and phenazine in biphenyl, respectively. Our results, 2.27 eV, 2.15 eV, and 3.22 eV for pentacene, 6,13-diazapentacene, and phenazine, respectively, indicate that we are able to a achieve a qualitative agreement with observations. In particular, the effect of nitrogen substitution (~0.1 eV decrease in excitation energy between pentacene and 6,13-diazapentacene) is well represented by our approach.

ISC. ISC transitions from S_1 to a nearby triplet state and the later transition from T_1 back to S_0 are essential processes for the organic room-temperature maser. As shown for benzene in Figure 1c, the lowest lying absorbing singlet state is not always the state of interest for the singlet–triplet ISC due to the existence of dark states between the ground and absorbing singlet state. In this case it is much more likely that the excited state will quickly decay to the S_1 state via IC rather than undergo ISC to the triplet manifold. Conceptually, this can be understood by noting that singlet–triplet transitions are spin forbidden while singlet–singlet (and triplet–triplet) transitions are not. In practice, this means that ISC rates are typically much slower than IC rates. This is also the case for 1,5-naphthyridine and 2,6-naphthyridine (see the Supporting Information); these must first relax to S_1 in order for ISC to the triplet manifold to occur.

Nonradiative transitions, both ISC and IC, are generally described by Fermi's golden rule (eq 1) which expresses the transition rate, k_{if}, between initial, i, and final, f, electronic states in terms of the electronic interaction matrix element, V_{if}, and the vibrational density of states of the final state, ρ_f.[48,49]

$$k_{if} = \frac{2\pi}{\hbar}|V_{if}|^2\rho_f \tag{1}$$

These nonradiative transitions are driven by the vibrational modes of the molecule.[49] We discuss two limiting cases: the so-called weak coupling and strong coupling limits. In the weak coupling limit, the energy surfaces of the two states do not intersect and the energies of the initial and final states, E_i and E_f, respectively, are separated by a large energy gap. In this case, an energy gap law can be formulated whereby the transition rate possesses an exponential (or superexponential) dependence on the energy gap.[50] In the strong coupling limit, the energy surfaces intersect for certain molecular arrangements and the transition rate possesses a Gaussian dependence on the energy gap between the two states and a Stokes shift term arising from molecular rearrangement of the molecule.

To discuss ISC rates, following the procedure by Simons,[49] the initial and final states are expressed as a mixture of singlet and triplet states using first order perturbation theory. That is, using

DOI: 10.1021/acs.jpcc.6b00150
J. Phys. Chem. C 2016, 120, 8251–8260

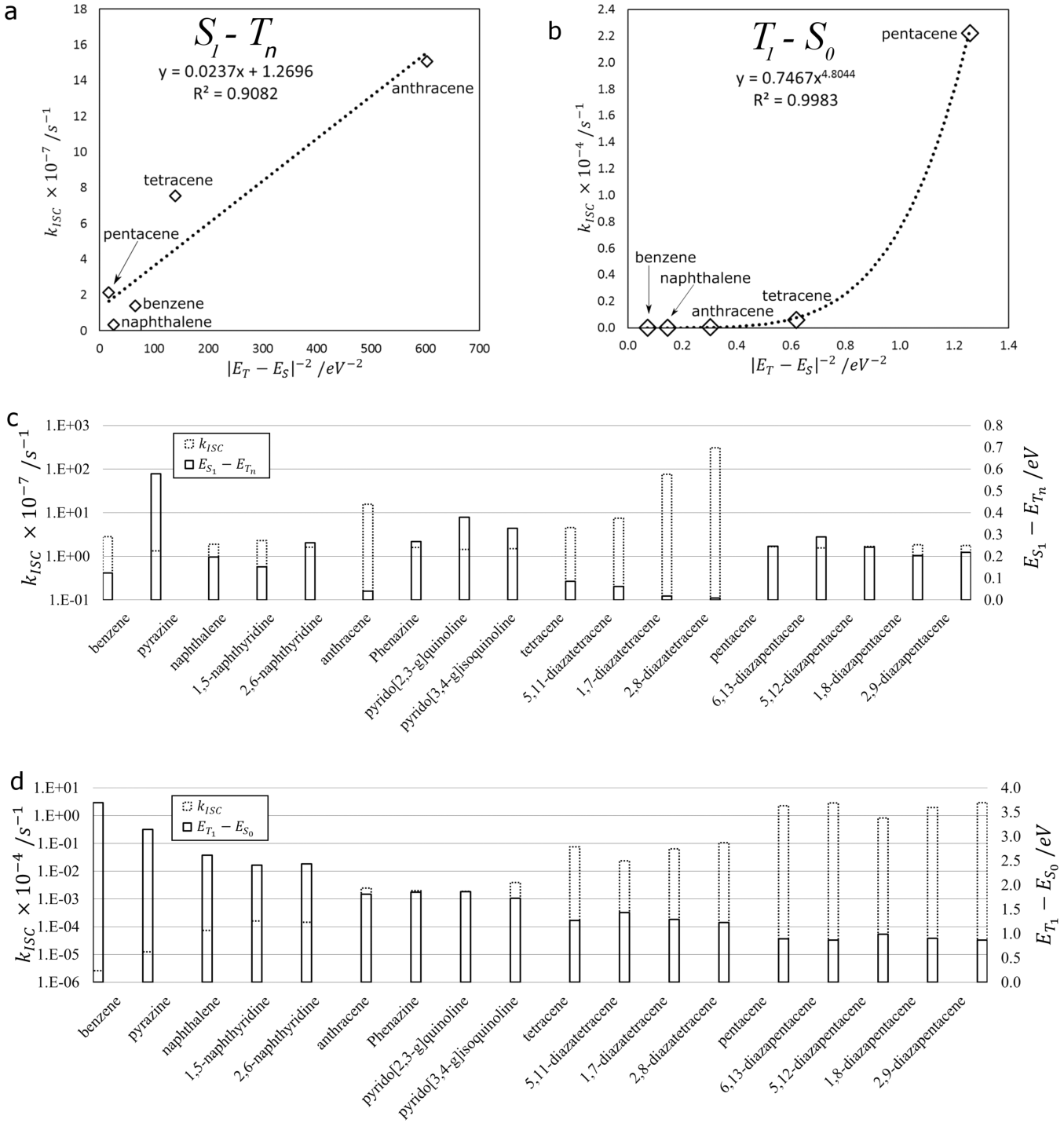

Figure 5. The S_1−T_n transition (a, c) and the T_1−S_0 transition (b, d). The inverse square of the energy gap, $|E_T-E_S|^{-2}$, computed between S_1 and the nearest downhill (energetically) triplet state, T_n, shows a rough correlation with observed ISC rates, $k_{ISC} \times 10^{-7}\ s^{-1}$, for the S_1−T_n transition (a) while a stronger correlation is observed for the T_1−S_0 ISC rates, $k_{ISC} \times 10^{-4}\ s^{-1}$ (b), where $|E_T-E_S|^{-2}$ is evaluated using the S_0 and T_1 energies. Singlet−triplet energy gaps for all molecules (estimated error is ∼0.2 eV for S_1−T_n and ∼0.03 eV for T_1−S_0, see the Supporting Information) and ISC rates for all candidate molecules estimated using eqs 4 and 5 are depicted in c and d for the S_1−T_n and T_1−S_0 transitions, respectively.

ϕ_{S_0} and ϕ_{T_1} as the initial wave functions for the S_0 and T_1 states, respectively, the $\tilde{\phi}_{S_0}$ and $\tilde{\phi}_{T_1}$ wave functions defined as

$$\tilde{\phi}_{S_0} = \phi_{S_0} + \langle \phi_{S_0} | h_{SO} | \phi_{T_1} \rangle (E_{S_0} - E_{T_1})^{-1} \phi_{T_1} \quad (2)$$

and

$$\tilde{\phi}_{T_1} = \phi_{T_1} + \langle \phi_{T_1} | h_{SO} | \phi_{S_0} \rangle (E_{T_1} - E_{S_0})^{-1} \phi_{S_0} \quad (3)$$

possess a mixture of T_1 and S_0 character, respectively, due to h_{SO}, the spin orbit coupling operator. The electron-interaction matrix element, $|V_{if}|^2$, in eq 1 thus contains spin−orbit coupling and an additional inverse square of the energy gap term. This does not necessarily improve the case of the weak coupling limit. However, in the case of a small energy gap (strong coupling) an inverse square of the energy gap dependence for the ISC rate

DOI: 10.1021/acs.jpcc.6b00150
J. Phys. Chem. C 2016, 120, 8251−8260

can be invoked. The reader is referred to the work of Simons[49] and of Engleman and Jortner[50] for a more thorough discussion.

In Figure 5a we compare our calculated S_1-T_n splittings to observed S_1-T_n ISC rates for the linear polyacenes. The choice of inverse square of the gap is motivated by the so-called energy gap law which in its simplest form states that k_{ISC} increases as the gap decreases (all other things being equal) and on the above-mentioned strong coupling limit. The results plotted in Figure 5a show a rough correlation between observed ISC rate[43] and calculated inverse square of the singlet−triplet splitting which is described by

$$k_{ISC} = \frac{0.0237\ \text{eV}^2\ \text{s}^{-1}}{|E_S - E_T|^2} + 1.2696\ \text{s}^{-1} \quad (4)$$

This may appear surprising because these transitions are also governed by spin−orbit coupling between the singlet and triplet states and the vibrational motion of the molecule in addition to the energy gap. However, it has been noted that the linear polyacenes possess similar spin−orbit coupling and vibrational structure.[44] The correlation with the S_1-T_n splitting suggests that ISC is dominated by resonance arising from relatively small S_1-T_n energy gaps. It is important to point out that we do not claim any physical significance to the slope ($0.0237\ \text{eV}^2\ \text{s}^{-1}$) and intercept ($1.2696\ \text{s}^{-1}$) that appear in Figure 5a. Rather, these are constants that have been obtained by comparing our specific DFT results to observations for the linear polyacenes. In Figure 5c we present the calculated S_1-T_n energy splittings and, using eq 4 as a predictive tool, the estimated ISC rates for the linear polyacenes and their diaza-substituted forms. It may be naively surmised that, because the π-structure is preserved under nitrogen substitution, the spin−orbit coupling is also occurring between qualitatively similar states. However, N-substitution has been shown to greatly enhance T_1-S_0 ISC rates via a mechanism whereby states are introduced that create a more efficient ISC channel.[44] Assuming similar arguments exist for the S_1-T_n ISC, the rates obtained using the equation defined in Figure 5a should be regarded as a novel tool for estimation of the S_1-T_n spin dynamics occurring in these compounds. Nonetheless, there appears to be tremendous value to this simple approach to gauging the S_1-T_n spin dynamics of potential maser materials with affordable amounts of computational work, which is the spirit of this study.

The S_1-T_n splittings and estimated S_1-T_n ISC rates (Figure 5c) display a large amount of variation with respect to nitrogen substitution. There does not appear to be a systematic trend describing the effect of nitrogen substitution, which prevents any qualitative mechanistic insight. However, the fact that both the S_0-S_1 (Figure 4) and T_1-S_0 (Figure 5d) transition energies display variation on the order of 0.1 eV with respect to nitrogen position clearly indicates that nitrogen substitution is affecting the S_1-T_n ISC rates via modulation of both the singlet and triplet manifolds. A wide range of gap energies and ISC rates are thus available indicating that nitrogen substitution is an attractive approach, from a materials engineering perspective, to achieve control of S_1-T_n ISC.

Based on these results we suggest that molecules with an S_1-T_n ISC rate which approaches or exceeds that of the pentacene in the *p*-terphenyl prototype are highly likely to function in a pulsed mode room-temperature maser. Surprisingly, this principle suggests that all candidates may operate as such. However, due to their similarity to the working prototype maser, the diazapentacenes (6,13-, 5,12-, 1,8-, and 2,9-diazapentacene) are especially likely to function in pulsed mode. The exceptionally high rates observed for anthracene, tetracene, and diaza-substituted forms of tetracene indicate promising candidates, all of which exhibit S_1-T_n ISC rates significantly faster than the working pentacene prototype. There remains, however, the task of supplying a suitable host crystal for these molecules.

Following ISC into the triplet manifold the system undergoes rapid IC to the lowest lying triplet state, T_1, after which a final T_1-S_0 ISC back to the singlet manifold brings the system to S_0. Our results for T_1-S_0 splitting and ISC rates are provided in Figure 5. A comparison between calculated T_1-S_0 splitting and observed ISC rates[44−46] for the linear polyacenes are provided in Figure 5b. The T_1-S_0 transition is well-known to be governed by vibronic coupling,[51] thus it is not surprising that the roughly linear correlation with $(E_S - E_T)^{-2}$ observed for the S_1-T_n ISC is not displayed for the T_1-S_0 ISC. However, a very good correlation is obtained from the following empirical equation.

$$k_{ISC} = 0.7467\ \text{eV}^{9.6088}\ \text{s}^{-1}\left(\frac{1}{|E_S - E_T|^2}\right)^{4.8044} \quad (5)$$

The calculated T_1-S_0 splittings and estimated T_1-S_0 ISC rates, calculated using eq 5, are provided in Figure 5d for the linear polyacenes and their diaza-substituted forms. The T_1-S_0 energy gaps and ISC rates appear to be well ordered with decreasing gap (increasing ISC rate) as polyacene length increases. Nitrogen substitution is playing an appreciable role in the T_1-S_0 ISC and, as mentioned above, appears to offer an attractive route for fine-tuning the spin-dynamics in these systems and in working toward a more efficient room-temperature maser.

To shed some light on how S_1-T_n and T_1-S_0 ISC rates influence CW maser operation, we have carried out a steady state population analysis of the T_1 triplet states (see Figure 6). The simplified model system we studied is provided in the inset to Figure 6 where populations of the S_0, S_1, and T_1 states are explicitly treated. The estimated population of T_1 is provided in Figure 6 as a function of an excitation rate, k_{ex}, which incorporates such properties as laser power, photon absorption efficiency, the density of masing molecules, and the rates of S_1-S_0 fluorescence and IC. The IC transition to T_1 from the higher lying triplet state, T_n, is assumed to be sufficiently fast such that the effective transition rate to T_1 can be approximated by the S_1-T_n ISC rate. The equation governing the population of T_1 under the steady state approximation is $T_1 = N/(1 + k_{TS}/k_{ex} + k_{TS}/k_{ST})$, where k_{ex}, k_{ST}, and k_{TS} are the excitation rates and S_1-T_n and T_1-S_0 ISC rates, respectively. The parameter N describes the number of maser molecules in the host matrix. For simplicity we set N to 1 and discuss the fraction of molecules in T_1. The equations governing the populations of the other states are provided in the Supporting Information. For each molecule there is a threshold excitation rate, k_{ex}, whereby occupation shifts from S_0 to T_1 indicated by the 0.5 contour value. In terms of maser operation: if the excitation rate is too low, then not enough spins are created (population of $T_1 \rightarrow 0$) and maser output will be too low; if the excitation rate is too high, then electrons will be promoted to the T_1 state (population of $T_1 \rightarrow 1$) faster than they can be returned to the ground state, again deteriorating CW maser operation. While a high excitation rate is well suited for a pulsed maser, indeed the maser prototype operates in pulsed mode, a CW maser requires a careful consideration of the rate at which the excited state manifolds are populated. From Figure 6, it follows intuitively that if the rate of population of T_1, k_{ST}, is sufficiently fast to allow for strong stimulated emission, then an excitation

DOI: 10.1021/acs.jpcc.6b00150
J. Phys. Chem. C 2016, 120, 8251−8260

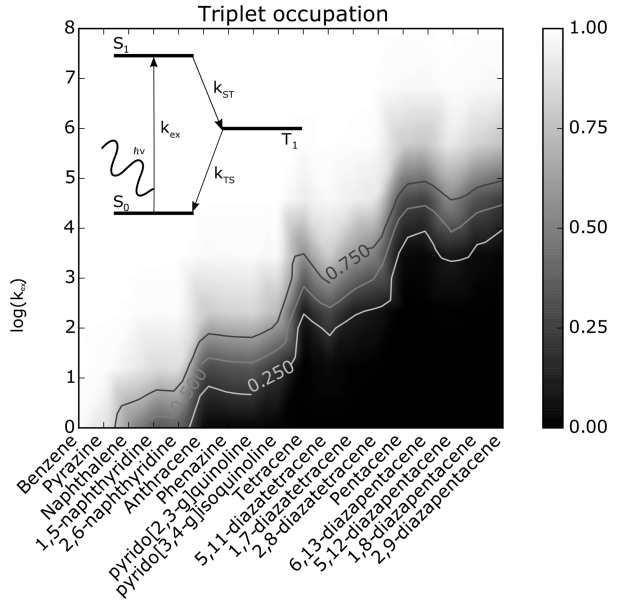

Figure 6. Population of the T_1 state under the steady state approximation for all molecules as a function of the excitation rate ($\log_{10}(k_{ex})$). The shading indicates values of k_{ex} (s^{-1}) for which the molecules tend to remain predominantly in the S_0 ground state (black) or the T_1 triplet state (white). S_1 population, not shown, remains small for all values of k_{ex}. Contour lines of 0.25, 0.50, and 0.75 are provided to more clearly identify regions where T_1 and S_0 populations are roughly equal and hence suggest the optimal operating conditions (as described by k_{ex}, see text) for CW masing.

rate, k_{ex}, that is not too fast nor too slow, relative to the T_1 decay rate, k_{TS}, would in principle induce continuous finite populations of T_1 and S_0 that should lead to CW operation. Based on these arguments it is reasonable to suggest that, in addition to pentacene, the molecules proposed for a pulsed mode room-temperature maser, that is, 6,13-, 5,12-, 1,8-, and 2,9-diazapentacene, tetracene, and its diaza-substituted forms and anthracene, should also, in principle, function as a CW maser.

Zero Field Splitting. The ZFS parameters D and E, which describe the splitting between T_Z and the midpoint between T_X and T_Y and between the states T_X and T_Y, respectively, were computed using the method developed by Neese and co-workers and implemented in the ORCA package.[25,26] The corrected D and E parameters (see the Supporting Information for further information) are presented in Figure 7.

The following general trends are observed: D values decrease with increasing acene length; E values increase from benzene to naphthalene and then decrease for anthracene, tetracene, and pentacene. The large D splitting calculated for 1,5-naphthyridine clearly violates this trend as do the large E values for pyrazine and 1,5-naphthyridine. The diaza-substituted forms do not appear to provide a strong influence on D splitting. The E splitting term, however, does indicate significant tunability of this splitting due to diaza substitution and hence control of the operational frequency of a VHF room-temperature maser[1] operating on transitions between T_X and T_Y.

Simulations of experimental EPR spectra measurements yield D = 1400 MHz and E = 50 MHz for pentacene in *p*-terphenyl, D = 1370 MHz and E = 85 MHz for 6,13-diazapentacene in *p*-terphenyl, and D = 2190 MHz and E = 326 MHz for phenazine in biphenyl. Our calculated values with the above-mentioned empirical correction are D = 1364 MHz and E = 37 MHz for pentacene in *p*-terphenyl, D = 1415 MHz and E = 117 MHz for 6,13-diazapentacene in *p*-terphenyl, and D = 2268 MHz and E = 360 MHz for phenazine in biphenyl. These are in reasonable agreement with experimental observations.

CONCLUSIONS

The exceptionally high S_1−T_n ISC rates (relative to pentacene) observed for the tetracene and its diaza-substituted forms (5,11-, 1,7-, and 2,8-diazatetracene) and for anthracene strongly suggest that these molecules be further studied for use in a room-temperature maser. Furthermore, based on their similarity to the pentacene in *p*-terphenyl prototype, all diaza-substituted forms of pentacene (6,13-, 5,12-, 1,8-, and 2,9-diazapentacene) studied are also suggested as targets for the room-temperature maser. While the diazapentacenes are compatible with the *p*-terphenyl host, optimal hosts for other compounds remain to be found. The possibility of achieving CW masing is demonstrated using a simple three state population model. We conclude that, provided the S_1−T_n ISC rate is sufficiently fast to populate the T_1 state, as predicted for the above-mentioned molecules, then an excitation rate, k_{ex}, exists such that continuous finite populations of T_1 and S_0 states are achieved. Provided these populations are established, CW masing would be in principle possible.

The S_1−T_n and the T_1−S_0 ISC transitions are inherently different and are found to be consistent with the strong-coupling

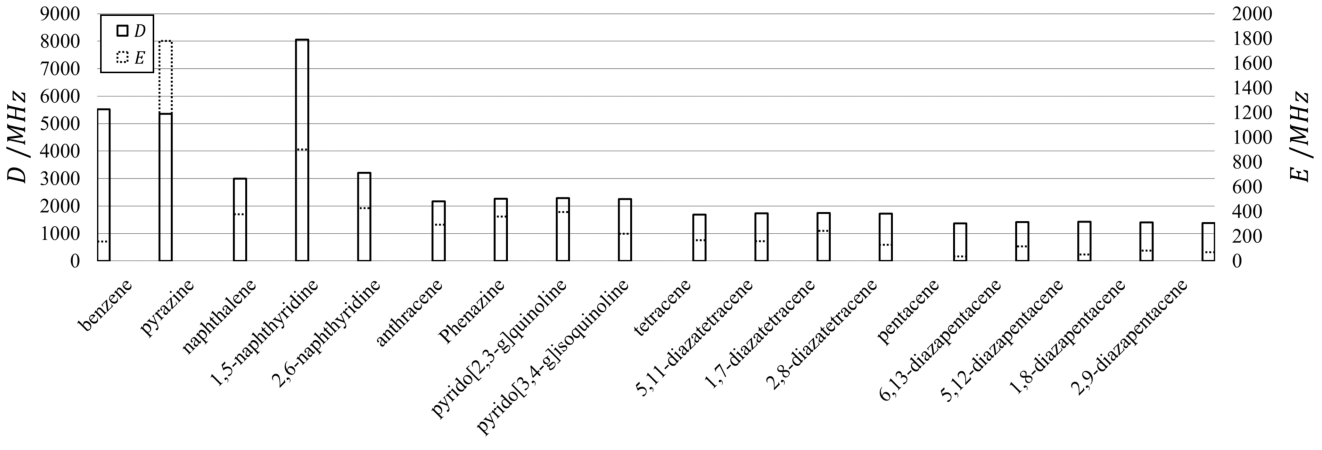

Figure 7. Zero field splitting (ZFS) parameters D and E of all molecules (estimated error ~30 MHz).

DOI: 10.1021/acs.jpcc.6b00150
J. Phys. Chem. C 2016, 120, 8251−8260

and weak-coupling limits, respectively, of the energy gap law described by Engleman and Jortner.[50]

Based on these ZFS parameters, operational frequencies (in MHz) of the recommended systems, i.e., tetracene, 5,11-diazatetracene, 1,7-diazatetracene, 2,8-diazatetracene, anthracene, 6,13-diazapentacene, 5,12-diazapentacene, 1,8-diazapentacene, and 2,9-diazapentacene, are 1853, 1893, 1993, 1855, 2464, 1532, 1477, 1485, and 1456, respectively, and 337, 321, 487, 260, 588, 235, 105, 169, and 141, respectively, in VHF mode. The strong influences of diaza substitution on E splitting is a route for fine-tuning the frequency of a VHF room-temperature maser.

■ ASSOCIATED CONTENT

Supporting Information

The Supporting Information is available free of charge on the ACS Publications website at DOI: 10.1021/acs.jpcc.6b00150.

Experimental details, tabulated results, and energy level diagrams (PDF)

■ AUTHOR INFORMATION

Corresponding Author

*E-mail: s.bogatko@ic.ac.uk.

Author Contributions

S.B. performed all DFT and TDDFT calculations. S.B., A.H, P.D.H., and M.O. designed the study. J.W., J.S., and J.-S.K. collected and analyzed the UV−vis absorption spectra. K.-J.T. carried out crystal growth. E.S. collected and simulated the EPR spectra. J.B. provided technical advice on the steady state population model. S.B. and A.H. wrote the paper with contributions from all authors.

Notes

The authors declare no competing financial interest.

■ ACKNOWLEDGMENTS

S.B. and A.H. thank the Leverhulme Trust for funding this work through grant RPG-2014-125, the Imperial College High Performance Computing Service for access to computational facilities, and the Thomas Young Centre for support under Grant TYC-101. E.S. gratefully acknowledges EPSRC for financial support, Grant Code EP/K011804/1. The authors thank Martin Heeney and Iain Andrews for synthesizing the 6,13-diazapentacene used in this study.

■ REFERENCES

(1) Oxborrow, M.; Breeze, J. D.; Alford, N. M. Room-Temperature Solid-State Maser. *Nature* **2012**, *488*, 353−356.

(2) Breeze, J.; Tan, K. J.; Richards, B.; Sathian, J.; Oxborrow, M.; Alford, N. M. Enhanced Magnetic Purcell Effect in Room-Temperature Masers. *Nat. Commun.* **2015**, *6*, 6215.

(3) Lin, T. S. Electron-Spin Echo Spectroscopy of Organic Triplets. *Chem. Rev.* **1984**, *84*, 1−15.

(4) Sloop, D. J.; Yu, H. L.; Lin, T. S.; Weissman, S. I. Electron-Spin Echoes of a Photo-Excited Triplet - Pentacene in Para-Terphenyl Crystals. *J. Chem. Phys.* **1981**, *75*, 3746−3757.

(5) Jin, L.; Pfender, M.; Aslam, N.; Neumann, P.; Yang, S.; Wrachtrup, J.; Liu, R.-B. Proposal for a Room-Temperature Diamond Maser. *Nat. Commun.* **2015**, *6*, 8251.

(6) Kraus, H.; Soltamov, V. A.; Riedel, D.; Vath, S.; Fuchs, F.; Sperlich, A.; Baranov, P. G.; Dyakonov, V.; Astakhov, G. V. Room-Temperature Quantum Microwave Emitters based on Spin Defects in Silicon Carbide. *Nat. Phys.* **2014**, *10*, 157−162.

(7) Clar, E. *Polycyclic hydrocarbons*; Academic Press: London, New York, 1964.

(8) Antheunis, D. A.; Schmidt, J.; van der Waals, J. H. Spin-Forbidden Radiationless Processes in Isoelectronic Molecules: Anthracene, Acridine and Phenazine. *Mol. Phys.* **1974**, *27*, 1521−1541.

(9) Zimmerman, P. M.; Zhang, Z. Y.; Musgrave, C. B. Singlet Fission in Pentacene Through Multi-Exciton Quantum States. *Nat. Chem.* **2010**, *2*, 648−652.

(10) Parr, R. G.; Yang, W. *Density-Functional Theory of Atoms and Molecules*; International series of monographs on chemistry; Oxford University Press; Clarendon Press: New York, Oxford, England, 1989.

(11) Marques, M. A. L.; Gross, E. K. U. Time-Dependent Density Functional Theory. *Annu. Rev. Phys. Chem.* **2004**, *55*, 427−455.

(12) Casida, M. E.; Huix-Rotllant, M. Progress in Time-Dependent Density-Functional Theory. *Annu. Rev. Phys. Chem.* **2012**, *63*, 287−323.

(13) Capelle, K. A Bird's-Eye View of Density-Functional Theory. *Braz. J. Phys.* **2006**, *36*, 1318−1343.

(14) Grimme, S.; Parac, M. Substantial Errors from Time-Dependent Density Functional Theory for the Calculation of Excited States of Large Pi Systems. *ChemPhysChem* **2003**, *4*, 292−295.

(15) Lopata, K.; Reslan, R.; Kowalska, M.; Neuhauser, D.; Govind, N.; Kowalski, K. Excited-State Studies of Polyacenes: A Comparative Picture Using EOMCCSD, CR-EOMCCSD(T), Range-Separated (LR/RT)-TDDFT, TD-PM3, and TD-ZINDO. *J. Chem. Theory Comput.* **2011**, *7*, 3686−3693.

(16) van Gastel, M. The Effect of Spin Polarization on Zero Field Splitting Parameters in Paramagnetic Pi-Electron Molecules. *J. Chem. Phys.* **2009**, *131*, 124111.

(17) Hohenberg, P.; Kohn, W. Inhomogeneous Electron Gas. *Phys. Rev.* **1964**, *136*, B864−B871.

(18) Kohn, W.; Sham, L. J. Self-Consistent Equations Including Exchange and Correlation Effects. *Phys. Rev.* **1965**, *140*, A1133−A1138.

(19) Perdew, J. P.; Burke, K.; Ernzerhof, M. Generalized Gradient Approximation Made Simple. *Phys. Rev. Lett.* **1996**, *77*, 3865−3868.

(20) Dunning, T. H. Gaussian-Basis Sets for Use in Correlated Molecular Calculations 0.1. The Atoms Boron through Neon and Hydrogen. *J. Chem. Phys.* **1989**, *90*, 1007−1023.

(21) Tomasi, J.; Mennucci, B.; Cammi, R. Quantum Mechanical Continuum Solvation Models. *Chem. Rev.* **2005**, *105*, 2999−3093.

(22) Selvakumar, S.; Murugaraj, R.; Viswanathan, E.; Sankar, S.; Sivaji, K. Dielectric Properties and Relaxation Mechanism of Organic Trans-Stilbene and p-Terphenyl Molecular Crystals Using Impedance Spectroscopy. *J. Mol. Struct.* **2014**, *1056*, 152−156.

(23) Tarasenko, O. Features of Charge Pairs Recombination in the Track Regions of Organic Solid Scintillators. *Funct. Mater.* **2012**, *19*, 421−428.

(24) Frisch, M. J.; Trucks, G. W.; Schlegel, H. B.; Scuseria, G. E.; Robb, M. A.; Cheeseman, J. R.; Scalmani, G.; Barone, V.; Mennucci, B.; Petersson, G. A.; et al. *Gaussian 09*, Revision D.01; Gaussian, Inc.: Wallingford, CT, 2009.

(25) Neese, F. The ORCA Program System. *WIREs-Comput. Mol. Sci.* **2012**, *2*, 73−78.

(26) Neese, F. Calculation of The Zero-Field Splitting Tensor on the Basis of Hybrid Density Functional and Hartree-Fock Theory. *J. Chem. Phys.* **2007**, *127*, 164112.

(27) Eichkorn, K.; Treutler, O.; Ohm, H.; Haser, M.; Ahlrichs, R. Auxiliary Basis-Sets to Approximate Coulomb Potentials. *Chem. Phys. Lett.* **1995**, *240*, 283−289.

(28) Hajgato, B.; Szieberth, D.; Geerlings, P.; De Proft, F.; Deleuze, M. S. A Benchmark Theoretical Study of the Electronic Ground State and of the Singlet-Triplet Split of Benzene and Linear Acenes. *J. Chem. Phys.* **2009**, *131*, 224321.

(29) Sinnecker, S.; Neese, F. Spin-Spin Contributions to the Zero-Field Splitting Tensor in Organic Triplets, Carbenes and Biradicalss - A Density Functional and Ab Initio Study. *J. Phys. Chem. A* **2006**, *110*, 12267−12275.

(30) Hashimoto, T.; Nakano, H.; Hirao, K. Theoretical Study of the Valence Pi- > Pi* Excited States of Polyacenes: Benzene and Naphthalene. *J. Chem. Phys.* **1996**, *104*, 6244−6258.

(31) Hiraya, A.; Shobatake, K. Direct Absorption-Spectra of Jet-Cooled Benzene in 130−260-nm. *J. Chem. Phys.* **1991**, *94*, 7700−7706.

DOI: 10.1021/acs.jpcc.6b00150
J. Phys. Chem. C 2016, 120, 8251−8260

(32) George, G. A.; Morris, G. C. The Intensity of Absorption of Naphthalene from 30 000 cm1 to 53 000 cm1. *J. Mol. Spectrosc.* **1968**, *26*, 67−71.
(33) Ferguson, J.; Reeves, L. W.; Schneider, W. G. Vapor Absorption Spectra and Oscillator Strengths of Naphthalene, Anthracene, and Pyrene. *Can. J. Chem.* **1957**, *35*, 1117−1136.
(34) Dick, B.; Zinghar, E.; Haas, Y. Spectral Hole-Burning of Tetracene and Tetracene Argon Complexes in a Supersonic Jet. *Chem. Phys. Lett.* **1991**, *187*, 571−578.
(35) Hartmann, M.; Lindinger, A.; Toennies, J. P.; Vilesov, A. F. The Phonon Wings in the (S-1 < - S-0) Spectra of Tetracene, Pentacene, Porphin and Phthalocyanine in Liquid Helium Droplets. *Phys. Chem. Chem. Phys.* **2002**, *4*, 4839−4844.
(36) Heinecke, E.; Hartmann, D.; Muller, R.; Hese, A. Laser Spectroscopy of Free Pentacene Molecules (I): The Rotational Structure of the Vibrationless S-1 < - S-0 Transition. *J. Chem. Phys.* **1998**, *109*, 906−911.
(37) Thompson, N. J.; Wilson, M. W. B.; Congreve, D. N.; Brown, P. R.; Scherer, J. M.; Bischof, T. S.; Wu, M. F.; Geva, N.; Welborn, M.; Van Voorhis, T.; et al. Energy Harvesting of Non-Emissive Triplet Excitons in Tetracene by Emissive PbS Nanocrystals. *Nat. Mater.* **2014**, *13*, 1039−1043.
(38) Vergragt, P. J.; Vanderwaals, J. H. Lowest Triplet-State of Benzene - Differences in Electronic-Structure in 2 Crystalline Modifications of a Cyclohexane Host. *Chem. Phys. Lett.* **1975**, *36*, 283−289.
(39) Hutchison, C. A.; Mangum, B. W. Paramagnetic Resonance Absorption in Naphthalene in Its Phosphorescent State. *J. Chem. Phys.* **1961**, *34*, 908−922.
(40) Grivet, J. P. Electron Spin Resonance of Phosphorescent Anthracene. *Chem. Phys. Lett.* **1969**, *4*, 104−106.
(41) Yu, H. L.; Lin, T. S.; Sloop, D. J. An Electron-Spin Echo Study of the Photo-Excited Triplet-State of Tetracene in Para-Terphenyl Crystals at Room-Temperature. *J. Chem. Phys.* **1983**, *78*, 2184−2188.
(42) Lang, J.; Sloop, D. J.; Lin, T. S. Dynamics of p-Terphenyl Crystals at the Phase Transition Temperature: A Zero-Field EPR Study of the Photoexcited Triplet State of Pentacene in p-Terphenyl Crystals. *J. Phys. Chem. A* **2007**, *111*, 4731−4736.
(43) Nijegorodov, N.; Ramachandran, V.; Winkoun, D. P. The Dependence of the Absorption and Fluorescence Parameters, the Intersystem Crossing and Internal Conversion Rate Constants on the Number of Rings in Polyacene Molecules. *Spectrochim. Acta, Part A* **1997**, *53*, 1813−1824.
(44) Clarke, R. H.; Frank, H. A. Triplet-State Radiationless Transitions in Polycyclic-Hydrocarbons. *J. Chem. Phys.* **1976**, *65*, 39−47.
(45) de Vries, H.; Wiersma, D. A. Fluorescence Transient and Optical Free Induction Decay Spectroscopy of Pentacene in Mixed-Crystals at 2-K - Determination of Intersystem Crossing and Internal-Conversion Rates. *J. Chem. Phys.* **1979**, *70*, 5807−5822.
(46) Hornburger, H.; Kono, H.; Lin, S. H. Excess Energy-Dependence in Radiationless Transitions - Triplet to Ground-State Nonradiative Rate Calculations in Benzene. *J. Chem. Phys.* **1984**, *81*, 3554−3558.
(47) Stoll, S.; Schweiger, A. EasySpin, a Comprehensive Software Package for Spectral Simulation and Analysis in EPR. *J. Magn. Reson.* **2006**, *178*, 42−55.
(48) Schatz, G. C.; Ratner, M. A. *Quantum Mechanics in Chemistry*; Dover Publications: Mineola, NY, 2002.
(49) Simons, J. *Energetic Principles of Chemical Reactions*; Jones and Bartlett: Boston, 1983.
(50) Englman, R.; Jortner, J. The Energy Gap Law for Radiationless Transitions in Large Molecules. *Mol. Phys.* **1970**, *18*, 145−164.
(51) Metz, F.; Friedrich, S.; Hohlneicher, G. What Is Leading Mechanism for Nonradiative Decay of Lowest Triplet-State of Aromatic-Hydrocarbons. *Chem. Phys. Lett.* **1972**, *16*, 353−358.

DOI: 10.1021/acs.jpcc.6b00150
J. Phys. Chem. C 2016, 120, 8251−8260